ACCSCIENCE PUBLISHING

Journal of Seismic Exploration

ARTICLE

Application of distributed helically wound cable technology in ground seismic exploration

Jingyuan Wang*, Bin Liu, Jing Zhu, and Weiwei Duan

Research and Development Center of Science and Technology, Sinopec Geophysical Corporation, Nanjing, Jiangsu, China

Abstract

Fiber optic distributed acoustic sensing (DAS) based on phase-sensitive optical time-domain reflectometry holds significant potential for monitoring applications in seismic exploration, pipeline integrity, and border security. Conventional straight-fiber DAS systems are inherently limited to detecting single-component vibration signals along the fiber axis. To address this limitation, we propose a distributed helically wound cable (HWC). In this article, we present a theoretical analysis of the fundamental mathematical model governing HWC response and the selection criteria for an optimal spiral wrapping angle. We conducted a pioneering three-dimensional seismic field experiment in Xinghua, Jiangsu, China. An innovative underwater cable deployment scheme was implemented to ensure effective coupling between the cable and the surrounding medium. Experimental results demonstrated that HWC with a 30° wrapping angle yielded single-shot records characterized by a high signal-to-noise ratio and a broad effective frequency bandwidth, and enabled clear identification of shallow reflection events in stacked sections. This confirms the capability of HWC to acquire ground seismic reflection signals. Our findings provide an effective pathway for advancing next-generation fiber optic distributed seismic exploration technology.

Keywords: Helical wound cable; Surface seismic exploration; Wrapping angle; Fiber optic sensing; Distributed acoustic sensing

***Corresponding author:**
Jingyuan Wang
(paixing3933@163.com)

Citation: Wang J, Liu B, Zhu J, Duan W. Application of distributed helically wound cable technology in ground seismic exploration. *J Seismic Explor*. doi: 10.36922/JSE025300040

Received: July 21, 2025

1st revised: August 15, 2025

2nd revised: August 25, 2025

Accepted: August 25, 2025

Published online: September 30, 2025

1. Introduction

Distributed optical fiber distributed acoustic sensing (DAS) technology is a new optical fiber sensing technology that uses optical fibers as sensors and achieves vibration signal acquisition based on Rayleigh scattering of light. It offers advantages including low cost, high measurement accuracy, immunity to electromagnetic interference, and ease of installation.[1,2] Compared to conventional single-point and quasi-distributed sensors, DAS is more suitable for long-distance or high-resolution applications in time and space, and is widely used in oil exploration, pipeline leak monitoring, and border security monitoring.[3,4]

Driven by the promise of cost reduction and increased channel density, significant research efforts in recent years have focused on adapting DAS technology for seismic applications that are traditionally dominated by geophones and accelerometers. Researchers have explored its use for microseismic event detection and localization,[5]

shallow near-surface characterization,[6] and vertical seismic profiling within boreholes,[7] and substantial progress has been made in fundamental theory, acquisition methodologies, processing algorithms, and interpretation techniques.[8,9] However, a persistent and fundamental challenge has hindered the widespread application of conventional DAS for surface seismic reflection surveys: its intrinsic directional sensitivity.

The underlying physics of phase-sensitive optical time-domain reflectometry-based DAS dictates that it is predominantly sensitive to strain components acting along the longitudinal axis of the optical fiber (axial strain), while exhibiting minimal response to strain perpendicular to this axis (radial strain).[10,11] Consequently, a straight optical fiber deployed horizontally on the surface acts as a highly directional sensor, primarily detecting seismic waves propagating along its length. This "single-component" nature is ideal for applications like vertical seismic profiling (where the fiber is near-vertical) or strain monitoring along pipelines. However, it renders standard DAS largely insensitive to the dominant energy arriving from near-vertical reflections in surface seismic exploration, where the fiber cable is typically laid horizontally, and the energetic reflected waves arrive almost perpendicularly to it. This critical mismatch in sensitivity direction has been the primary barrier preventing DAS from replacing conventional geophone arrays for land seismic acquisition.

To overcome this fundamental limitation of axial-strain-only sensitivity, Hornman *et al.*[12] pioneered the concept of the helically wound cable (HWC). The core innovation involves coiling the sensing optical fiber into a helical structure around a central strength member or mandrel within the cable jacket. This geometric transformation is pivotal; when seismic waves impinge on the cable, inducing complex strains within its structure, the helical path of the fiber ensures that its local axis has significant components in both the radial and tangential directions relative to the cable's cross-section. As a result, the fiber experiences strain components related to both compressional waves (P-waves; causing volume changes) and shear waves (S-waves; causing transverse particle motion). This multi-component sensitivity significantly enhances the DAS system's responsiveness to the diverse wave types and arrival directions encountered in surface seismic exploration, making its application in this domain theoretically feasible. Wuestefeld and Wilkd[13] advanced the understanding by employing precise ray tracing in complex velocity models to determine wave incidence angles and further elucidated the intricate relationships between subsurface medium properties, the mechanical properties of the DAS cable's wrapping materials, and the optimal helical wrapping angle for maximizing signal fidelity.[13] Furthermore, Innanen[14] developed sophisticated mathematical models for helical fibers wound along arbitrarily curved axes, specifically addressing the challenges of strain tensor estimation and the reconstruction of P-wave and S-wave signals from the measured DAS data.[14,15] These models have also been instrumental in forward modeling and inversion studies of seismic elastic waves using DAS data.[16-18] Despite these significant theoretical and simulation advances, rigorous experimental validation of HWC performance under realistic field conditions, particularly through direct comparison with established geophone arrays in three-dimensional (3D) seismic surveys, remains relatively scarce and represents a crucial research gap that needs bridging for technology maturation.

To directly address the core limitation of standard straight-fiber DAS for surface seismic—its inability to capture near-vertical reflections—this study focuses on the development, theoretical underpinning, and comprehensive field testing of a distributed HWC system designed explicitly for land seismic exploration. Based on a detailed theoretical analysis of the fundamental mathematical model governing strain transfer in helical fibers under seismic excitation, an optimal spiral wrapping angle was selected to maximize sensitivity to vertically incident waves while ensuring robust performance across a range of angles. We then conducted a pioneering 3D seismic field experiment in Xinghua, Jiangsu, China, implementing a novel underwater deployment strategy to ensure effective cable-medium coupling—a critical factor often challenging to achieve with conventional trenching or surface-laid methods, especially for kilometer-scale cables. The primary objective was to empirically evaluate the HWC's ability to acquire genuine surface seismic reflection signals, assess its data quality relative to conventional nodal systems, and validate its practical feasibility for next-generation seismic acquisition.

2. Design and theoretical analysis of a distributed HWC

In oil and gas exploration applications, distributed optical cables function as sensors to detect weak seismic waves. When a light pulse propagates along the optical fiber core, Rayleigh scattering occurs due to inhomogeneities within the fiber. The system detects the backward-scattered Rayleigh light, generating an interference pattern. When external forces such as sound pressure act on the optical cable, the optical fiber will be strained, and the interference image will change. By detecting the change, the amplitude of the seismic wave can be reconstructed. As compressional waves (P-waves) are predominantly used in seismic exploration and generate strain parallel to their propagation direction, this study focuses on P-waves

as the research object. If a plane P-wave propagates along the D-axis, then the unique non-zero strain component along this axis is denoted as $e^{(w)}$. Suppose the optical cable is oriented at an angle θ with respect to the D-axis, as shown in Figure 1. The direction of e_z is parallel to the axial direction of the fiber, and the direction of $e_{\|}$ is parallel to the axial direction of the optical cable. Strain $e^{(w)}$ is a second-order tensor, and its component $e_{\|}^{(w)}$ along the parallel direction of the optical cable length is $e^{(w)}\cos^2\theta$. If the fiber is well coupled with the optical cable, the optical cable is well coupled with the external structural layer, and there is no loss at the contact interface, then $e_{zz}^{(f)} = e_{\|}^{(c)} = e^{(w)}$, i.e., the strain of the fiber is proportional to $\cos^2\theta$, independent of the optical cable material and the external structural layer parameters.

Based on the effect of seismic P-wave on the linear optical cable, the optical fiber is wound as shown in Figure 2. The optical fiber is tightly wound on the surface of the cylindrical optical cable shaft, cut along the direction AB of the left figure, and expanded to get the right figure. The wrapping angle α of the optical fiber is the angle between the optical fiber and the radial direction of the optical cable.

Suppose $b = |AB|$ in Figure 2, the circumference of the fiber wrapping cylinder, is $\alpha = 2\pi R$, and R is the radius of the cylinder, then the diagonal L of the rectangle on the right is the length of the fiber (**Equation I**):

$$\frac{\Delta L}{L} = \frac{a}{L^2}\frac{\Delta a}{a} + \frac{b^2}{L^2}\frac{\Delta b}{b} \tag{I}$$

When the optical cable generates strain under the action of seismic waves, its cross-section will become an ellipse. Let b_1 and b_2 be the length of the long axis and short axis of the ellipse, respectively, then the ellipse equation can be obtained as follows (**Equation II**):

$$\begin{Bmatrix} x = b_1\cos\beta \\ y = b_2\cos\beta \end{Bmatrix} \tag{II}$$

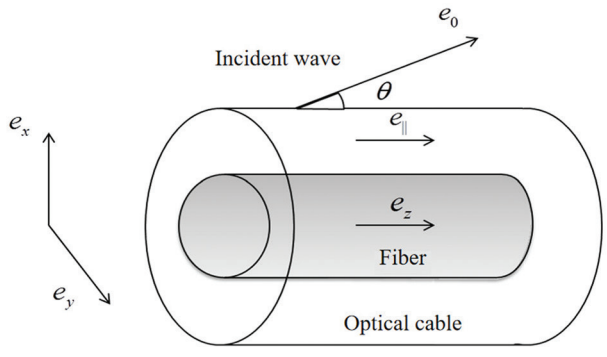

Figure 1. Schematic diagram of the effect of seismic waves on optical cables.

The circumference of the ellipse is $\tilde{a} = \pi(b_1 + b_2)2\pi\tilde{R}$, where $\tilde{R}$ is the approximate radius of the ellipse, $\Delta a / a = \Delta R - R$, and $\Delta R = \tilde{R} - R$, then **Equation I** can be expressed as **Equation III**:

$$e_{ZZ}^{(ff)} = e_{\|}^{(c)}\sin^2\alpha + \left\langle e_{rr}^{(c)}\right\rangle\cos^2\alpha \tag{III}$$

where α is the wrapping angle, $e_{ZZ}^{(ff)} = \frac{\Delta L}{L}$ is the axial strain of the optical fiber, $e_{\|}^{(c)} = \frac{\Delta b}{b}$ is the axial strain of the optical cable, $\left\langle e_{rr}^{(c)}\right\rangle = \frac{\langle \Delta R\rangle}{R}$ is the radial strain of the optical cable, cos α = a/L, and sin α = b/L.

This relationship can be derived as follows (**Equation IV**):

$$e_{ZZ}^{(f)} = e_{\|}^{(w)}\sin^2\alpha + \frac{(\lambda+2N)e^{(w)} - (\lambda_c+2N)e_{\|}^{(w)}}{2(\lambda_c+N_c+N)}\cos^2\alpha \tag{IV}$$

The internal strain of the loaded wave is taken as the unit strain, that is, $e^{(w)} = 1$. According to the previous analysis, $e^{(w)} = \cos^2\theta$ can be expressed as follows (**Equation V**):

$$e_{ZZ}^{(f)} = \cos^2\theta\sin^2\alpha + \frac{(\lambda+2N)e^{(w)} - (\lambda_c+2N)e_{\|}^{(w)}}{2(\lambda_c+N_c+N)}\cos^2\alpha \tag{V}$$

According to **Equation V,** the strain of the spiral fiber is related not only to the Lamme coefficient of the fiber and optical cable, but also to the wrapping angle and the incidence angle of the seismic wave. Without considering the fiber and optical cable material, the simplified **Equation V** can be obtained through **Equation VI**:

$$e_{ZZ}^{(f)} = \cos^2\theta\sin^2\alpha + \frac{1}{2}\cos^2\theta\cos^2\alpha \tag{VI}$$

According to **Equation VI**, when the wrapping angle of the fiber is constant, the relationship between the relative

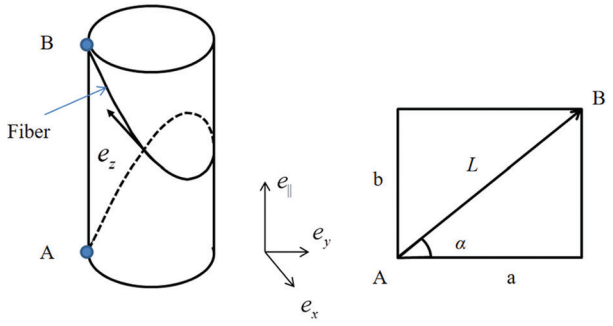

Figure 2. Schematic diagram of the distributed fiber wrapping.

fiber strain and the incidence angle of the seismic wave is shown in Figure 3. For the incident wave of the same angle, different wrapping angles will produce different optical fiber strains, and for the same wrapping angle, different angle incident waves will also produce different optical fiber strains. When α is 90°, the optical fiber is linear, the sensitivity is minimal, and the angle of incidence has the greatest influence on the relative strain. When α is 0°, the relative fiber strain is large, that is, the sensitivity is high, and the consistency is also affected by the incident angle. When the wrapping angle α is about 30°, the sensitivity is relatively large, and the consistency of the relative strain of the fiber is good.

To identify the optimal wrapping angle, we analyzed angles between 27° and 36° in 2° increments (Figure 3). At a wrapping angle of 33°, the fiber exhibits not only high sensitivity but also minimal variation in strain response across different incident angles.

According to **Equation VI**, the relationship between relative fiber strain and fiber wrapping angle is shown in Figure 4 when the incident angle is constant. When the incident angles are 0°, 20°, 40°, 60°, and 80°, there are two intersection points between 0 ~ π in the fiber wrapping angle, and the effect of the two intersection points on the fiber strain is the same. If one of the points is selected, its radius is 0.58; hence, the angle is 33°, and the strain generated at this point is the same for different incident angles. Thus, it has the same strain response characteristics.

3. High-definition (HD) distributed optical fiber acoustic wave sensing technology

HD-DAS is implemented based on the principle of self-coherent heterodyne demodulation,[19,20] with its schematic diagram as shown in Figure 5A. The system uses the optical signal modulation module to modulate the continuous light emitted by the ultra-narrow linewidth laser into a pair of pulses, where the two pulse frequencies are f_1 and f_2, respectively, and the heterodyne frequency is $\Delta f = f_1 - f_2$. The pulses are first amplified by the optical amplifier, and then injected into the sensing fiber through the circulator. The Rayleigh backscattered signal in the fiber reaches the signal detection module through the circulator and is then demodulated through the demodulation module for the heterodyne algorithm to obtain the phase change of the light wave caused by the external sound field. The system does not need the interference of Rayleigh scattering and local light, and the scattered light of the two pulses will interfere with each other to achieve a self-coherent effect. Then, the phase change caused by the external sound wave is modulated to the heterodyne frequency, and the high-precision phase signal can be obtained by a heterodyne demodulation algorithm. In addition, given that the noise environment experienced by the double pulse is the same, the common mode noise can be eliminated to a large extent after self-coherence, and the system can obtain a good noise background. Figure 5B shows the assembled HD-DAS system engineering prototype. Table 1 shows the specific technical specifications of the HD-DAS system.

4. Data acquisition

4.1. Acquisition of geometry design

The HWC seismic acquisition test was conducted within a 3D survey area located in Xinghua City, Jiangsu. The acquisition utilized a single-point high-density 3D geometry. The receiver array consisted of I-nodal and SmartSolo nodal units. The seismic source consisted of 3D explosive charges deployed in shot holes at 12 m depth with a shot interval of 40 m; a total of 100 shots were fired. The HWC receiver line (total length: 2 km) was positioned 200 m away from the shot line.

To extend the spatial coverage for comparative analysis, the HWC receiver array was repositioned three times as the shot points advanced. Each repositioning involved moving the HWC forward by 1 km. After three movements, seismic data covering a total profile length of 5 km were acquired (Figure 5).

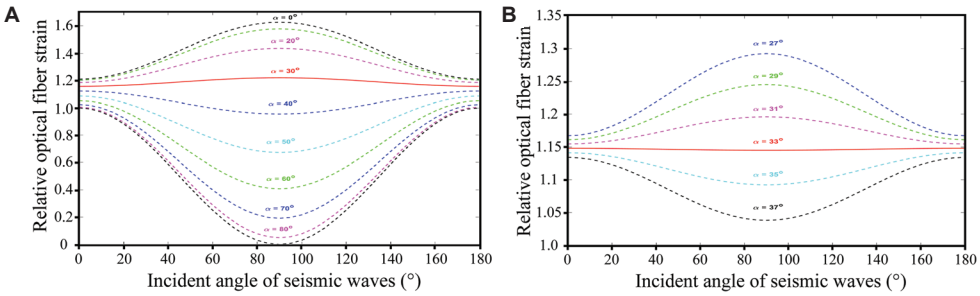

Figure 3. R elative optical fiber strains. Relation between relative fiber strain and (A) incidence angle and (B) local magnification.

Based on the theoretical analysis presented in Section 2 (Figures 3 and 4), a wrapping angle of approximately 30°–33° is identified as optimal for achieving high sensitivity to vertically incident waves while maintaining good angular response consistency. However, manufacturing HWC with a precise 30° wrapping angle presents significant process challenges and higher costs compared to angles closer to the natural lay of fibers, such as 60°. Theoretically, a 60° wrapping angle is expected to exhibit inferior acquisition performance, particularly for vertical waves. To quantitatively assess the impact of this parameter on field data quality and evaluate the viability of 60° HWC, the 2 km cable was constructed with two distinct segments: (i) an 860 m segment with a 60° wrapping angle, and (ii) a 1,140 m segment with a 30° wrapping angle.

In the receiver array layout, the 30° and 60° segments were concatenated into a single cable spanning the survey line, with the 30° segment occupying the northern 1,140 m (Traces 1–1,140) and the 60° segment the southern 860 m (Traces 1,141–2,000) (Figure 6). This placement ensured that data from segments with different wrapping angles were acquired under identical geological conditions, source characteristics, and near-surface effects. Directly comparing data quality between these segments under comparable field conditions provides an unambiguous assessment of the wrapping angle's impact on acquisition fidelity.

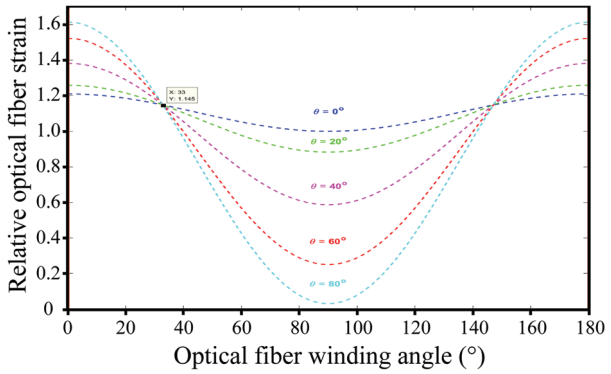

Figure 4. The relationship between the relative fiber strain and the fiber wrapping angle.

4.2. Deployment of HWC

Effective mechanical coupling between the HWC and the surrounding geological medium is paramount for high-quality seismic data acquisition. Poor coupling acts as a low-pass filter, attenuating high-frequency signal components, and introduces spurious noise, severely degrading signal-to-noise ratio and resolution. Common HWC deployment methods for surface seismic include:

(i) Trenching: Excavating deep trenches (typically >0.5 m) using machinery and burying the cable, providing good coupling but at high cost and environmental impact.

(ii) Surface laying: Placing the cable directly on the ground surface. This is logistically simple but results in very poor coupling efficiency and high susceptibility to

Table 1. High-definition distributed optical fiber acoustic wave sensing system technical specifications

Index item	Technical index value
Noise background ($dB\ ref\ rad/\sqrt{HZ}$)	−80
Stress resolution ($p\varepsilon/\sqrt{HZ}$)	2.5
Measurement bandwidth (kHz)	2
Spatial resolution (m)	1
Scale length (m)	8
Dynamic range (dB)	>100
Sensing distance (m)	50~2,500

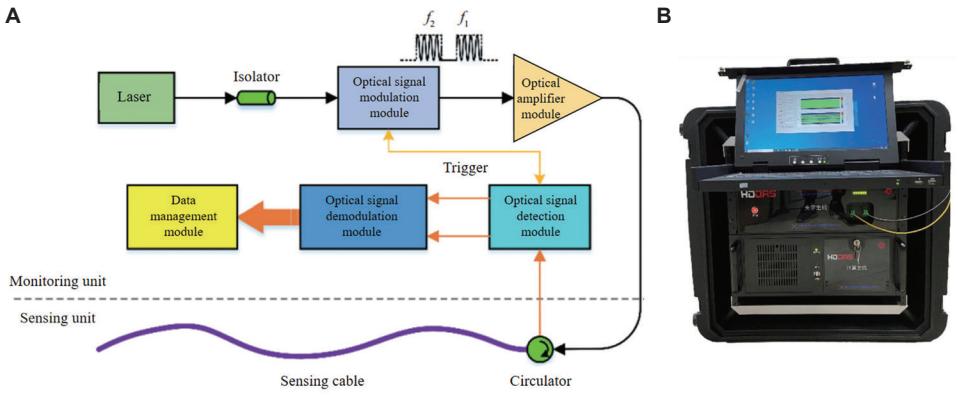

Figure 5. System overview and implementation. (A) High-definition distributed optical fiber acoustic wave sensing system principle and (B) engineering prototype.

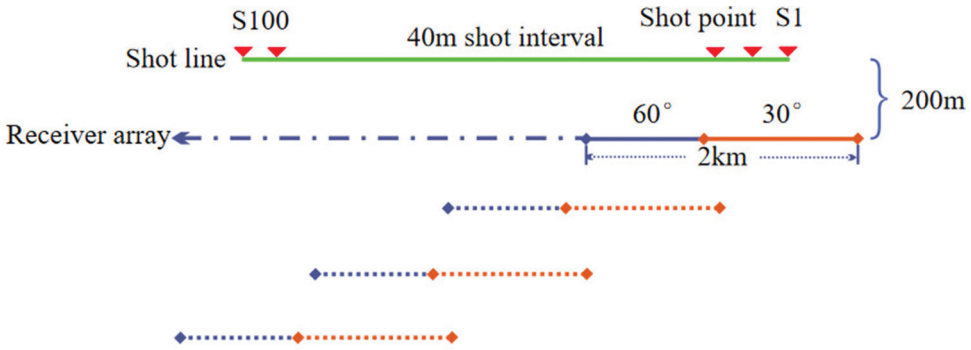

Figure 6. Schematic diagram of the helically wound cable acquisition geometry.

ground roll, wind noise, and cultural noise, leading to significantly degraded data quality.

While trench burial has been used in some international HWC trials, its applicability is often limited to relatively short cable lengths (typically <600 m in reported studies) due to the prohibitive cost and time required for excavating and reinstating long trenches. Given the 2 km length of our HWC and the requirement for three repositionings (totaling 5 km of cable deployment), conventional trench burial was deemed economically and logistically impractical.

To overcome this critical challenge and ensure effective coupling for the entire length of the cable during all deployment phases, we designed and implemented an innovative underwater deployment scheme. The HWC was carefully laid on the riverbed along the section parallel to the seismic line (Figure 7). Water provides excellent coupling due to its incompressibility and efficiently transmits seismic P-waves propagating as acoustic waves. Crucially, these acoustic waves in water fully retain the reflected P-wave information from subsurface structures, despite the difference in propagation velocity compared to the solid earth. This principle is supported by the theory of Ainslie,[21] which demonstrates that the dynamics of P-waves in fluids are analogous to those in solid media (lacking only the shear component), aligning perfectly with our objective of P-wave acquisition (Section 2.1). Repositioning the 2 km cable for the roll-along acquisition was efficiently achieved using a small tugboat (Figure 7), significantly reducing deployment time and cost compared to trenching.

5. Data analysis and results

5.1. Single-shot analysis

Figure 8A compares shot gathers acquired simultaneously by the 30° and 60° HWC segments. A significant performance contrast was evident: the left section (30° HWC) displayed recognizable seismic signals, particularly in shallow layers, despite interference from ground roll and other noise.

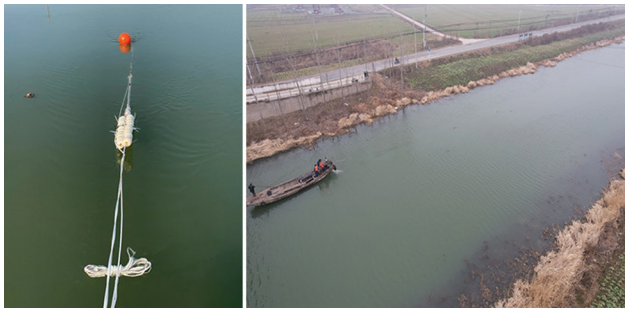

Figure 7. Field deployment documentation of helically wound cable.

Conversely, the right section (60° HWC) was severely contaminated by noise, resulting in a critically low signal-to-noise ratio that renders effective wave identification nearly impossible. Spectral analysis (Figure 8B) provided quantitative confirmation of the 30° segment's superiority. The amplitude spectrum of the 30° HWC data showed higher amplitudes across a broader frequency range than the 60° segment. Crucially, the 30° HWC demonstrated a significantly broader effective bandwidth, preserving more high-frequency content essential for achieving higher seismic resolution. The 60° segment's spectrum exhibited noticeable attenuation, particularly at higher frequencies, and lower overall energy, consistent with its noisy time-domain character.

The superior quality of the 30° HWC data enabled comparison with nodal acquisition. Comparison with nodal acquisition revealed key differences. The 30° HWC gather exhibited stronger ground roll amplitudes but weaker first arrivals compared to the nodal data, highlighting distinct sensor sensitivities and radiation patterns that warrant further investigation into coupling effects. Due to the shorter receiver spread length (2 km) and finer trace interval (1 m) of the HWC array, reflection hyperbolas appeared significantly flatter than those in the nodal gather. This fine spatial sampling is a key DAS advantage for high-resolution imaging, particularly of shallow, steeply dipping events.

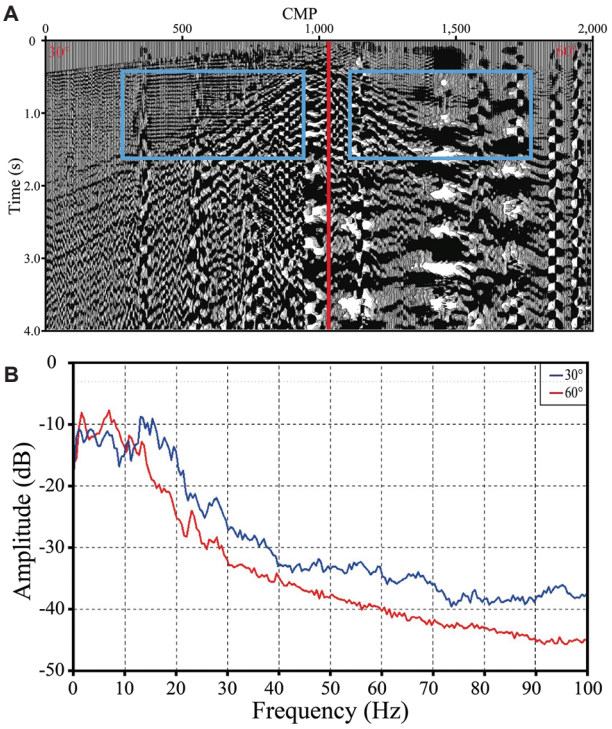

Figure 8. Performance comparison of shot gathers from different wrapping angles. (A) Shot records and (B) spectral analysis.
Abbreviation: CMP: Common midpoint.

Frequency-band scanning of the shot records (Figure 9) showed that effective reflection wave energy for both systems occupied a similar band (5–60 Hz). While waveform characteristics differed—likely due to sensor response, coupling, and directional sensitivity variations—the fundamental similarity in detected frequency content confirms both systems captured primary subsurface reflections. The HWC data showed good coherence within each filtered band, comparable to the nodal data.

5.2. Profile analysis

Given the extremely poor data quality of the 60° HWC segment (Figure 8A), incorporating it into the full processing flow would severely degrade the final stacked section. Consequently, we applied a split processing strategy during data conditioning. Data from the 30° and 60° sections were processed separately. While this isolation preserved the integrity of the 30° signals, it introduced significant compromises:

(i) Reduced fold coverage: The effective spread length contributing to any common midpoint bin was reduced (utilizing only the 30° or 60° segment, not the full 2 km cable).
(ii) Spatially inconsistent coverage: Fold coverage became highly variable along the profile, dropping sharply at the boundaries between segments and remaining low within each segment compared to the nodal array.
(iii) Dead trace zones: Some common midpoint bins, particularly at segment boundaries or due to the roll-along geometry, received zero coverage ("dead traces"), creating gaps in the stacked section (Figure 10 illustrates the discontinuous coverage).

Stacked profile comparisons between the 60° and 30° HWC segments (Figure 10) revealed significant differences. In the 60° stacked section (Figure 10A), reflection events were identifiable only in isolated, very shallow zones (likely corresponding to strong, near-surface reflectors). Throughout the vast majority of the section, reflection signals were scarcely discernible above the background noise. The overall data quality was markedly inferior, confirming the severely limited capability of the 60° HWC to effectively capture reflected wave energy under these field conditions. The theoretical prediction of inferior performance is strongly validated.

The 30° stacked section (Figure 10B), despite processing challenges (low/uneven fold, gaps), showed clear improvement. Continuous reflection events with reasonably coherent wave group characteristics were identifiable, particularly at shallow-to-intermediate depths (down to 1.0–1.5 s two-way time. This demonstrates the fundamental capability of the optimally designed 30° HWC to acquire coherent surface seismic reflections and produce a meaningful subsurface image, even under suboptimal acquisition conditions.

To further validate HWC feasibility, we compared the stacked profile from the 30° HWC segment with a nodal array profile acquired concurrently. The nodal profile benefited from single-point high-density acquisition and a fold coverage exceeding 800. The HWC profile faced inherent limitations: a short total cable length (2 km), separate processing of segments reducing effective spread length, and the roll-along geometry, resulting in extremely uneven fold coverage with a maximum of only 55.

Despite a significantly lower fold, the 30° HWC profile (Figure 11A) displayed clear reflection events with reasonably continuous wave groups. The fine 1-meter trace spacing of the HWC provides superior vertical and horizontal resolution in the shallow section compared to the nodal profile. However, the limited maximum offset (~1.4 km) resulted in weaker mid-to-deep section reflections. Nevertheless, reflection events consistent with the nodal profile were observable in the mid-to-deep section (ellipse, Figure 11A), though with weaker amplitudes and poorer continuity, constrained by the

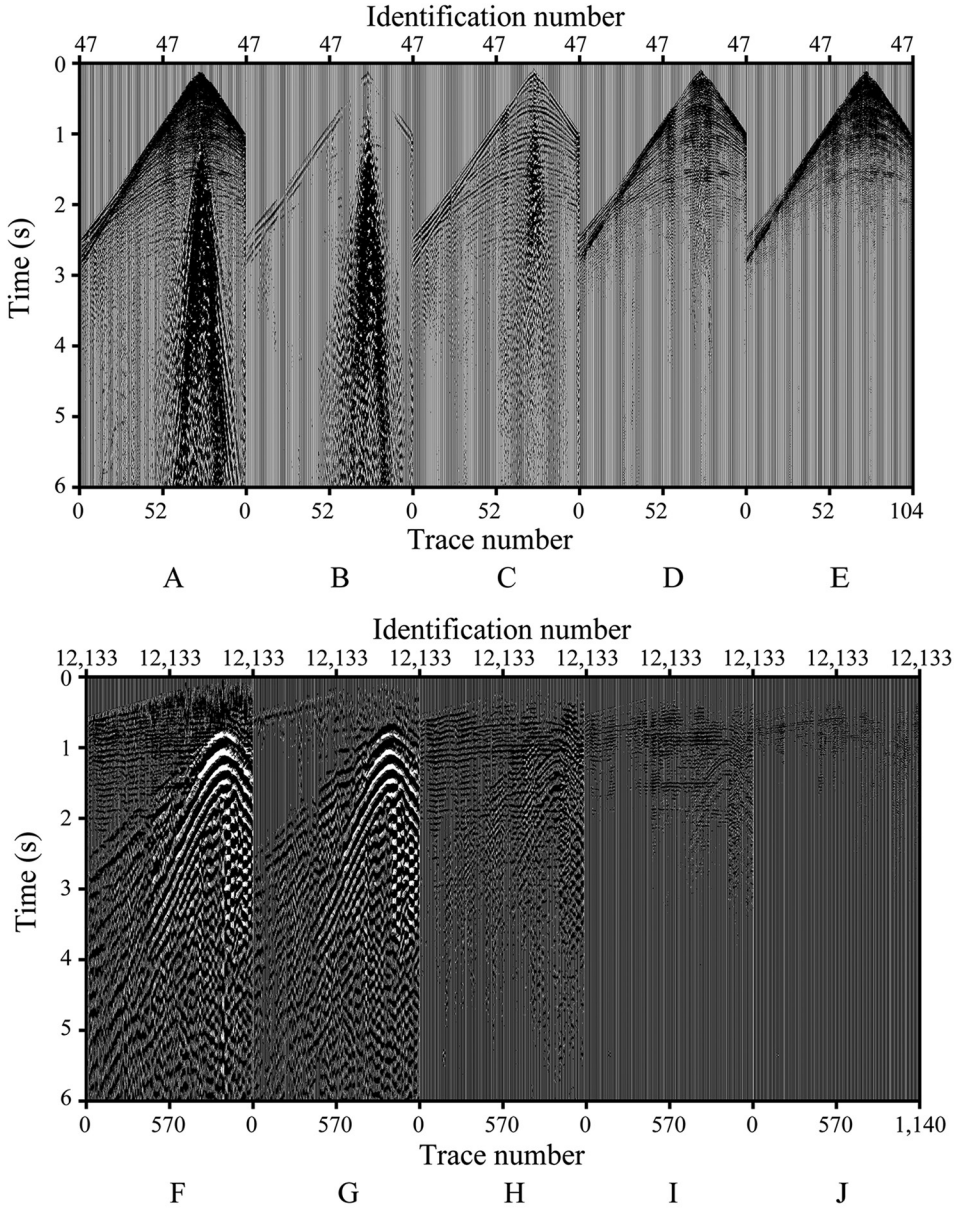

Figure 9. Frequency-band scanning comparison of shot gathers with (A-E) nodal acquisition and (F-J) 30° HWC acquisition. (A and F) Raw shot gather; (B-G) 5–10Hz; (C–H) 10–20Hz; (D–I) 20–40Hz; (E-J) 0–60Hz.

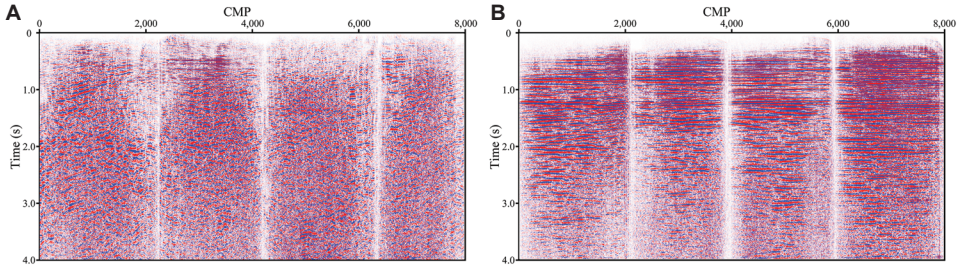

Figure 10. Performance comparison of seismic acquisition methods: (A) 60° HWC and (B) 30° HWC.
Abbreviations: CMP: Common midpoint; HWC: Helically wound cable.

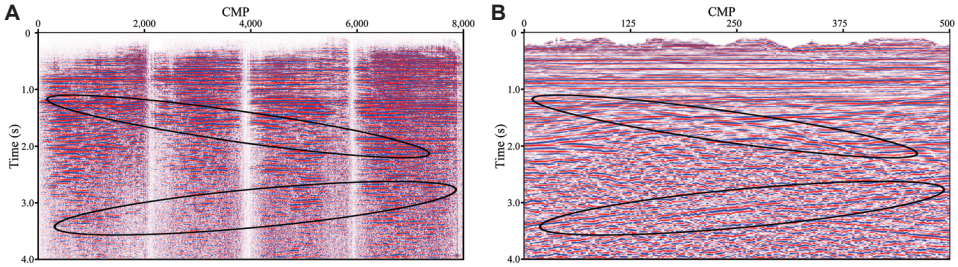

Figure 11. Performance comparison of seismic acquisition methods: (A) the HWC acquisition profile and (B) the seismic profile. Abbreviations: CMP: Common midpoint; HWC: Helically wound cable.

low/uneven fold and limited offsets. Overall, the HWC demonstrated a clear capability to acquire surface seismic reflection data, showing significant practical potential.

6. Discussion

While this study demonstrates significant promise, it also highlights areas for further development. The current limitations in fold coverage and maximum offset inherent in our test setup impacted the mid-to-deep section quality. Future work should focus on deploying longer HWC arrays or multiple parallel cables to achieve sufficient fold and offset distribution for robust imaging of deeper targets. Quantitative comparisons of signal fidelity, resolution, and noise characteristics between HWC and geophones with matched fold conditions are needed. Furthermore, developing specialized processing flows tailored to HWC DAS data, particularly addressing its unique noise fields, amplitude behavior, and directional sensitivity, will be crucial for maximizing its potential. From an economic viewpoint, considering cable manufacturing costs, deployment efficiency, and operational scalability compared to large nodal arrays requires a detailed assessment as the technology advances. Nevertheless, this successful field trial marks a substantial step forward. Distributed HWC technology, with its unique combination of high-density sampling, operational flexibility in challenging environments, and proven ability to capture surface seismic reflections, offers a compelling pathway for next-generation seismic acquisition systems aimed at higher resolution, lower cost, and reduced environmental footprint.

7. Conclusion

This study proposed and field-tested an HWC for DAS in land seismic exploration. Combining theoretical analysis with field experimentation, we optimized the HWC design and evaluated its performance, yielding the following key conclusions. To overcome the single-component (axial) sensitivity limitation of conventional straight-fiber DAS, we developed the HWC concept. Helically winding the sensing fiber enhances sensitivity to both compressional (P-) and shear (S-) waves, significantly expanding DAS applicability to surface seismic exploration. Field data acquired with optimally wound (30°) HWC exhibited clear seismic signals, continuous wave groups, and high resolution (particularly shallow), demonstrating its viability for practical surface seismic acquisition. Deploying HWC cables in challenging terrains, such as water networks and tidal flats, through our innovative underwater scheme effectively resolved coupling issues. This approach leverages the inherent advantages of high spatial sampling density offered by DAS and eliminates the problem of missing traces encountered when deploying conventional geophones in inaccessible areas.

Acknowledgments

None.

Funding

This study was financially supported by the Sinopec Project "Development and Pilot Test of Distributed Spiral Optical Fiber Sensing System" (Grant No. SGC-2024-21).

Conflict of interest

The authors declare they have no competing interests.

Author contributions

Conceptualization: Jingyuan Wang, Bin Liu
Formal analysis: Jing Zhu, Weiwei Duan
Investigation: Bin Liu,Jing Zhu
Methodology: Jingyuan Wang, Weiwei Duan
Visualization: Jing Zhu, Weiwei Duan
Writing–original draft: Jingyuan Wang, Bin Liu
Writing–review & editing: All authors

Availability of data

All data analyzed have been presented in the paper.

References

1. Wang C, Shang Y, Zhao WA, *et al.* Investigation and comparison of Φ-OTDR and OTDR-interferometry via

phase demodulation. *IEEE Sens J*. 2018;18(4):1501-1505.

doi: 10.1109/JSEN.2017.2785358

2. Shi Y, Feng H, Zeng ZM. Distributed fiber sensing system with wide frequency response and accurate location. *Opt Lasers Eng*. 2016;77:219-224.

doi: 10.1016/j.optlaseng.2015.08.010

3. Du QC, Wang C, Shang Y, *et al*. Study on distributed fiber seismic wave detection system and its layout optimization. *Shandong Sci*. 2017;30(5):55-61.

doi: 10.3976/j.issn.1002-4026.2017.05.010

4. Lin TF, Dou LR, Gan LD. Development history and prospect of seismic exploration technology. *World Pet Ind*. 2023;30(1):57-69.

doi: 10.20114/j.issn.1006-0030.2023.01.012

5. Song ZH, Zeng XF, Xu SH, Hu JP, Sun TW, Wang BS. Distributed acoustic sensing for imaging shallow structure I: Active source survey. *Chin J Geophys*. 2020;63(2):532-540.

doi: 10.6038/cjg2020N0184

6. Sui WB, Liu RQ, Cui K. Application and research progress of distributed optical fiber acoustic sensing monitoring for hydraulic fracturing. *Sci Sin Technol*. 2020;51(4):1622-1629.

doi: 10.1360/SST-2020-0195

7. Li YP, Li F, Li JG, Jin QH, Liu CW, Wu JJ. Application of distributed acoustic sensing in borehole seismic exploration. *Geophys Prospect Petroleum*. 2020;59(2):242-249.

doi: 10.3969/j.issn.1000-1441.2020.02.007

8. Mestayer J, Karam S, Cox B, *et al*. Distributed Acoustic Sensing for Geophysical Monitoring. In: *Expanded Abstracts of 74th EAGE Conferenceand Exhibition*; 2012. p. 4253-4557.

doi: 10.3997/2214-4609.20148800

9. Zhou R. Development status and prospect of optical fiber seismic wave detection technology. *Sci Technol Innov*. 2020;(3):15-16.

10. Cao DP, Lv JJ, Sun SR, Ma GQ, Yin JJ. Three-componet signal acquisition mechanism of distributed acoustic sensing based on helically winding fiber-optic. *Geophys Prospect Pet*. 2022;61(1):60-69.

doi: 10.3969/j.issn.1000-1441.2022.01.006

11. Hornman JC. Field trial of seismic recording using distributed acoustic sensing with broadside sensitive fibre-optic cables. *Geophys Prospect*. 2017;65(1):35-46.

doi: 10.1111/1365-2478.12358

12. Hornman K, Kuvshinov B, Zwartjes P, Franzen A. Field Trial of a Broadside-Sensitive Distributed Acoustic Sensing Cable for Surface Seismic. In: *Expanded Abstracts of 75th EAGE Conference and Exhibition*.

13. Wuestefeld A, Wilkd M. How to twist and turn a fiber: Performance modeling for optimal DAS acquisitions. *Leading Edge*. 2019;38(3):226-231.

doi: 10.1190/tle38030226.1

14. Innanen KA. Parameterization of a Helical DAS Fibre Wound about an Arbitrarily Curved Cable Axis. In: *79th EAGE Conference and Exhibition*. Vol. 1; 2017. p. 1-5.

doi: 10.3997/2214-4609.201701202

15. Innanen KA. Determination of Seismic-Tensor Strain from Helical Winding Cable-Distributed Acoustic Sensing Cable with Arbitrary and Nested-Helix Winds. In: *Expanded Abstract of 87th Annual Internat SEG MTG*; 2017. p. 926-930.

16. Eaid MV, Li JX, Innanen KA. Modeling the Response of Shaped DAS Fibres to Microseismic Moment Tensor Sources. In: *Expanded Abstracts of 88th Annual Internat SEG MTG*; 2018. p. 4698-4702.

doi: 10.1190/segam2018-2998378.1

17. Eaid MV, Keating SD, Innanen KA. Multi-parameter seismic elastic full waveform in version with combined geophone and shaped fiberoptic cable data. *Geophysics*. 2020;85(6):1-66.

doi: 10.1190/geo-2020-0170.1

18. Egorov A, Correa J, Bona A, *et al*. Elastic full-waveform inversion of vertical seismic profile data acquired with distributed acoustic sensors. *Geophysics*. 2018;83(3):273-281.

doi: 10.1190/geo2017-0718.1

19. He XG, Pan Y, You HJ, *et al*. Fibre optic seismic sensor for down-well monitoring in the oil industry. *Measurement*. 2018;123(1):145-149.

doi: 10.1016/j.measurement.2018.03.047

20. He XG, Zhang M, Gu LJ, Xie SR, Liu F, Lu HL. Performance improvement of dual-pulse heterodyne distributed acoustic sensor for sound detection. *Sensors*. 2020;203(4):999.

doi: 10.3390/s20040999

21. Ainslie MA, McColm JG. A simplified formula for viscous and chemical absorption in sea water. *J Acoust Soc Am*. 1998;103(3), 1441-1445.

doi: 10.1121/1.421258